

Hydrodynamic Swarming of Thermally Active Dimeric Colloids

Martin Wagner¹ and Marisol Ripoll¹

¹*Theoretical Soft-Matter and Biophysics, Institute of Complex Systems,
Forschungszentrum Jülich, 52425 Jülich, Germany*

(Dated: November 13, 2018)

Self-propelled phoretic colloids have recently emerged as a promising avenue for the design of artificial swimmers. These swimmers combine purely phoretic interactions with intricate hydrodynamics which critically depend on the swimmer shape. Thermophobic dimer shaped colloids are here investigated by means of hydrodynamic simulations, from the single particle motion to their collective behavior. The combination of phoretic repulsion with hydrodynamic lateral attraction favors the formation of planar moving clusters. The resulting hydrodynamic assembly in flattened swarms is therefore very specific to these dimeric active colloids.

PACS numbers: 66.10.cd, 87.17.Jj, 05.70.Ln, 02.70.Ns

Synthetic microscale motors are attracting large attention due to their outstanding potential practical applications in fields like microfluidics or microsurgery [1–3]. When the propulsion mechanism is based on phoretic effects [4], such artificial microswimmers have the great advantage of behaving like passive colloids unless they are chemically [1, 5, 6], electrically [7, 8], or thermally activated [9–11]. In particular, thermophoretic swimmers are built from two materials with well differentiated absorption coefficients, like gold and silica, where heterogeneous heating can produce a steady local temperature gradient around the colloid, which translates into its persistent self-propulsion. Thermophoretic swimmers can therefore be powered without any modification of the solvent, what makes them easily bio-compatible. Furthermore, devices engineered with this effect are expected to depict a very large versatility due to two additional facts. One is that thermophoresis has shown to be very sensitive to a large number of factors like pressure, average temperature or solvent composition; and two is that the heat sources, such as magnets or lasers, can be very precisely controlled in time and space.

Large ensembles of phoretic swimmers are expected to share a large number of properties with other systems of active particles. Chemically active Janus colloidal particles have already shown clustering and self-assembled structures [12] as well as schooling behavior; and the formation of living crystals has already been observed for light powered micromotors [13, 14]. Brownian simulations of thermophilic active colloids predicted the appearance of clustering and comet-like swarming structures [15, 16]. Nevertheless, the mechanisms involved in the formation of these structures, the importance of the phoretic and hydrodynamic effects, and the behavior of various types of phoretic swimmers are still very relevant and largely unexplored questions. Until now, spherical Janus thermophoretic swimmers have been the only geometry investigated experimentally [9, 17, 18], although important effects related with particle shape can be expected. Catalytic dimer motors, moving in the direction

of the catalytic cap, have already been synthesized [6]. These results indicate that diffusio- and thermophoretic motion of dimeric colloids in both directions are experimentally feasible.

In this letter we investigate thermophobic dimer shaped colloids by means of computer simulations. Thermophobic colloidal behavior is much more frequent than thermophilic one. Furthermore, these active colloids constitute a paradigmatic case in which the interplay of phoretic repulsion and hydrodynamic attraction results in spontaneous self-assembly of oriented and collectively moving structures, reminiscent of planar order. These remarkable swarming structures appear then to be specific to phoretic active colloids; their direction of motion will be easier to control [19] such that promising applications are to be expected, as those related to directed cargo transport [20] or the development of microfluidic devices [21, 22].

Simulations are performed with a hybrid mesoscopic approach. Multiparticle collision dynamics (MPC) is the particle based method used to describe the fluid, and molecular dynamics (MD) is employed to describe the colloids and the colloid-fluid interactions [23, 24]. This description has shown to properly incorporate hydrodynamic interactions, also in phoretic systems [25–27]. MPC describes the fluid as a collection of point particles of mass m that perform alternating streaming and collision steps. In the streaming step, particles propagate ballistically for a time h . In the collision step, the particles are binned into cells of side length a . A grid shifting procedure [28] is employed during this binning to ensure Galilean invariance. Inside the collision cells, the particles velocities relative to the center-of-mass velocity of the cell are rotated around a random axis by an angle α . The choice of $a = 1$, $m = 1$ and $k_B \bar{T} = 1$ defines the simulation units, so that time is scaled with $\sqrt{ma^2/k_B \bar{T}}$ and velocity with $\sqrt{k_B \bar{T}/m}$. The other parameters are here chosen to be $\alpha = 120^\circ$ and $h = 0.1$, together with the averaged number of particles per collision cell, $\rho = 10$.

These numbers determine the fluid transport properties as the solvent Schmidt number, which here is $Sc = 13$, or the fluid kinematic viscosity $\nu = 0.79$.

Colloid-fluid interactions are modelled with MD, and the choice of the potential is crucial to determine phoretic and collective properties of the colloids. Thermophobic behavior has been observed with attractive interactions, and thermophilic with repulsive ones [29]. On the other hand, a pronounced depletion interaction between colloids might occur as result from the high compressibility of the MPC fluid [30]. A detailed investigation shows this effect to be very pronounced when using steep attractive potentials [31]. The colloid-fluid potential $U(r)$ and related parameters are then chosen to avoid such artificial depletion in the system. We use displaced Lennard-Jones-type potentials given by

$$U(r) = \begin{cases} \infty, & r \leq \Delta \\ 4\varepsilon \left[\left(\frac{\sigma}{r-\Delta} \right)^{48} - \left(\frac{\sigma}{r-\Delta} \right)^{24} \right] + C, & \Delta < r < r_c \\ 0, & r_c \leq r \end{cases} \quad (1)$$

Here r is the pairwise distance, ε describes the strength of the potential which we choose as $\varepsilon = k_B \bar{T}$, and Δ introduces a displacement. Repulsive interactions are obtained with $C = \varepsilon$ and $r_c = 2^{1/24} \sigma + \Delta$, and attractive with $C = 0$ and $r_c = 1.13 \sigma + \Delta$. With this model, the effective radius of each bead is $s = \sigma + \Delta$, and we denote the related size parameters as (s, Δ) . Dimers investigated here are constructed by one phoretic bead with attractive interactions of size s_P , which we fix as $(6, 3)$; and one hot bead with repulsive interactions of size s_H , which we mostly fix as either $(6, 3)$ or $(2, 0.5)$. Both beads are held together by a strong harmonic potential at a distance $s_H + s_P$. Similar to previous works [10, 32], heating is modeled by rescaling the temperature of fluid particles in a short layer ($0.08 s_H$) around the hot beads to a value of $T_h = 1.5$, while keeping the overall average fluid temperature at $\bar{T} = 1.0$ using simple velocity rescaling. This constant heating neglects shadowing effects [16], it corresponds to colloids made of materials with the same light refraction index as the solvent, and which in the case of thermophobic behavior will have smaller influence. Simulations are performed using a modified variant of the software package LAMMPS [33], in particular a modified version of the 'srd'-package [34]. The time-step to integrate the potential interactions is $\Delta t = 0.01 h$, and the bead mass is chosen such that the swimmers are neutrally buoyant.

Besides the employed colloid-fluid interactions, the swimmer dimensions importantly influence both the swimmer velocity and hydrodynamic behavior. Given a constant temperature gradient, the size of the phoretic bead will determine the phoretic thrust, which will be larger, the larger the bead [29, 35]. In this study the size of the phoretic bead is fixed to $s_P = 6$. The sym-

metric swimmer with $s_H = s_P$ shows a propelled velocity against the heated bead with an averaged value of $v_s = 0.021$, which corresponds a Reynolds number $Re = v_s s / \nu = 0.32$, where the relevant particle size is $s = s_H + s_P$. At such low Reynolds numbers, inertial effects can be neglected and Stokes hydrodynamic behavior is to be expected. Increasing the size of the heated bead increases the temperature gradient around the phoretic bead, such that the phoretic thrust is larger, but it also increases the overall friction of the swimmer. The combination of these two effects results in a maximum of the propelled swimmer velocity as a function of the size ratio $\gamma = s_P / s_H$ of the two dimer beads as can be seen in Fig. 1a. The dimer velocity is measured in the main dimer axis towards the phoretic bead. The simulations were performed for single swimmers in a cubic periodic box of side length $10(s_H + s_P)$. The bead size ratio of the dimer also changes its rotational diffusion coefficient which we have measured for $\gamma = 1$ as $D_r = 2.5 \times 10^{-5}$ and for $\gamma = 3$ as $D_r = 1.2 \times 10^{-4}$, what allows us to determine the Peclet number $Pe = v_s / (s D_r)$ of both swimmers as 70 and 20 respectively. These dimensionless numbers are comparable, and even a bit higher than those of experimentally synthesized spherical Janus swimmers [9, 36].

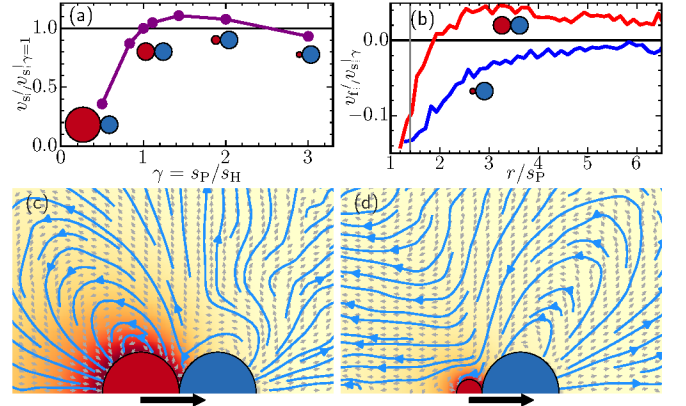


Figure 1: a) Single swimmer velocity v_s as a function of the bead size ratio γ normalized by the velocity of the symmetric swimmer, $v_s|_{\gamma=1}$. b) Fluid velocity v_f as a function of r , the distance to the center of the phoretic bead in the axis perpendicular to the swimmer orientation. The normalizing factor $v_s|_{\gamma}$ is the corresponding single swimmer velocity. Vertical grey line is the minimum distance from the phoretic bead center to the surface of another dimer. Blue (dark) lines stand for symmetric dimers and red (light) for asymmetric dimers. c) Flow field characterization in the area close to the symmetric dimer $\gamma = 1$. Solid lines correspond to the stream lines, background color depicts the temperature field, and grey arrows show the direction of the fluid velocity. Black thick arrow indicate the dimer swimming direction. d) Flow field close to the asymmetric dimer $\gamma = 3$, with symbols similar to c).

The swimmer shape also influences strongly the hydrodynamic response of the surrounding fluid. The quantitative values of the flow velocities in the axis perpendicular

to the swimmer orientations is depicted in Fig. 1b, and the stream lines around the two thermophoretic dimers are displayed in Figs. 1c,d. Negative values of the velocity correspond to fluid streaming towards the bead (*hydrodynamic attraction*), while positive values correspond to the fluid streaming away from the bead (*hydrodynamic repulsion*). The dimers flow fields are of the point force-dipole type [37, 38], whose precise form strongly depends on the geometry of the swimmer. The symmetric dimer, with $\gamma = 1$, shows mainly hydrodynamic lateral repulsion, although there is a small region close to the phoretic bead where attractive interactions also exist. This qualitatively changes in the case of asymmetric dimers, with $\gamma = 3$, which show strong and long ranged lateral hydrodynamic attraction. This can be seen in Fig. 1d, where the stream lines show a large attractive lobe close to the phoretic bead, and in Fig. 1b where the fluid velocity is clearly negative over the whole range of accessible distances.

The described hydrodynamic behavior, combined with the thermophobic character of the dimers, strongly suggests that the collective dynamics of these dimers will be different from each other and from other synthetic swimmers [14, 39]. To characterize the collective dimer dynamics, we performed simulations with $N = 100$ swimmers at a volume fraction of $\phi = 0.05$ for thermophobic swimmers of both size ratios. This number of swimmers is limited by the employed large bead diameters, which implies the use of up to 4×10^7 MPC fluid particles. Colloid-colloid strong repulsive interactions are considered between all i, j beads of different dimers, by using potentials corresponding to Eq. (1) with $\Delta = 0, \varepsilon = 2.5k_B\bar{T}$, and $C = \varepsilon$. The interaction distance is $\sigma = 1.2(s_i + s_j)$, which includes a small additional separation to resolve lubrication forces [30] and to avoid residual depletion while maintaining the hydrodynamic interactions.

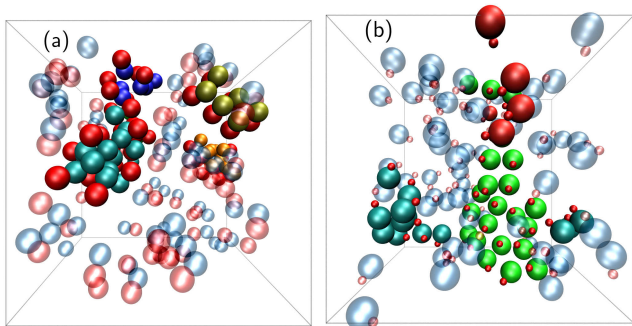


Figure 2: Snapshots of ensembles of thermophoretic dimers. a) Symmetric swimmers ($\gamma = 1$). b) Asymmetric swimmers ($\gamma = 3$). Non-assembled dimers are translucent, with red heated beads and blue phoretic beads. Dimers assembled in clusters of size five or larger are solid, with red heated beads and phoretic beads colored according to cluster identity. See related movies [40].

Thermophobic dimers with the two considered symmetries have a very dynamic behavior, constantly assembling and de-assembling in clusters of various sizes. Snapshots illustrating different kinds of behavior are shown in Fig. 2, and two representative movies can be found in [40]. In Fig. 2a, four clusters of symmetric dimers can be distinguished, the two blue ones are randomly jammed structures, resulting from collisions of various dimers or existing smaller clusters, swimming in random directions. The other two clusters show clear orientational order, which will be necessarily accompanied by a significant average velocity. The light green cluster of asymmetric dimers in Fig. 2b shows a distinct large planar and oriented structure, with certain hexagonal order, which will collectively move as a front. The strong lateral hydrodynamic attraction favors asymmetric dimers to swim close and aligned to other dimers, and the phoretic repulsion avoids the proximity of other dimers in their axial direction, resulting in the planar structures. Although the two described assembling mechanisms, hydrodynamics or collisions, are present for both symmetric and asymmetric swimmers, the hydrodynamic is clearly more important for the asymmetric ones. In the case of the symmetric dimers the clusters are small-sized and short-lived, while asymmetric dimers form considerably larger and faster clusters with a pronounced tendency to be planar aligned, which can propel over one to several dimer lengths. These swarming clusters are in strong contrast with the observed behavior of spherical diffusiophoretic colloids in quasi-2D confinement [14, 39], or squirmer-type swimmers [41] with attractive interactions, which crystallize in large static clusters.

To better quantify these effects we perform a cluster analysis of our simulation results. Any two dimers with beads i, j closer than $1.32(s_i + s_j)$ (this is 1.1 times the colloid-colloid minimum interaction distance) are considered to belong to the same cluster. Figure 3a displays the probability of a dimer to be part of a cluster of size N_c . Although most dimers are part of very small clusters, it can be seen that for symmetric dimers a significant fraction of them assembles in clusters of up to $\approx 20\%$ of the swimmers; meanwhile asymmetric dimers show to assemble in significantly larger clusters that might reach over 50% of the swimmers in the system. In our discussion, we do not consider data from cluster sizes with a probability below 10^{-3} , since they can be considered rare events. Note that once a cluster is formed, the number of constituent dimers is strongly fluctuating, since single dimers are constantly attaching and detaching, and the cluster is easily dividing and merging with others. An indication of the most typical cluster sizes can then be found in the plateaus of the probability function in Fig. 3a, which indicates $N_c = 15$ for $\gamma = 1$ and $N_c = 45$ for $\gamma = 3$. The cluster velocity along the main cluster direction is plotted in Fig. 3b. The main cluster direction is obtained by averaging all single dimer axes \vec{n}_i ,

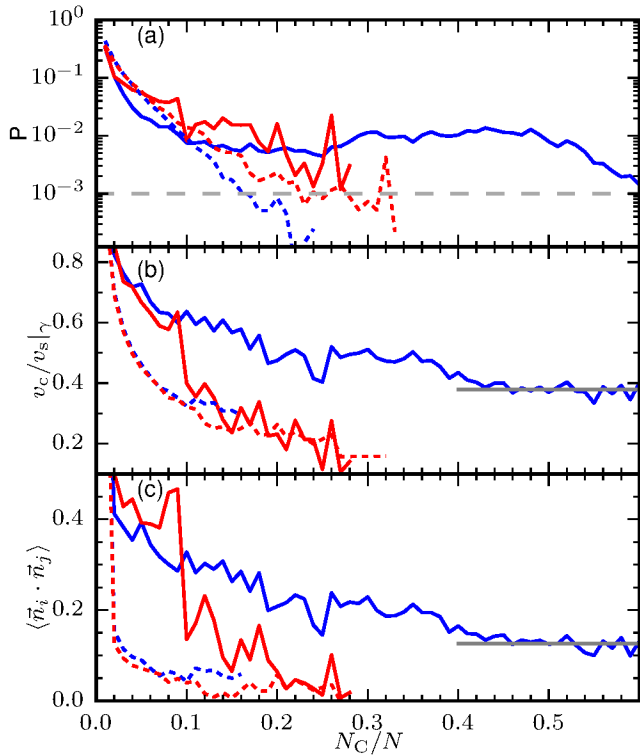


Figure 3: a) Averaged probability for a dimer of being in a cluster of normalized size N_C/N . Blue (dark) lines stand for symmetric dimers and red (light) for asymmetric dimers. Solid lines correspond to hydrodynamic simulations (MPC-MD), dashed lines to non-hydrodynamic results (LD). Gray dashed line shows the probability threshold. b) Normalized cluster velocities as a function of normalized cluster size. c) Orientational correlation of dimers within the same cluster as a function of the normalized cluster size. b,c) Solid gray lines are a guide to the eye indicating a saturation value.

and the cluster velocity is the average of the dimer velocities projected on such cluster direction. The average correlation of all dimer orientations in a cluster $\langle \vec{n}_i \cdot \vec{n}_j \rangle$ is shown in Fig. 3c. For symmetric dimers, the velocity and the orientation clearly decay with cluster size, and although significant propulsion velocity and orientation is found for small clusters, both are almost vanishing for the largest clusters of symmetric dimers, as expected for jammed structures. For asymmetric dimers, velocities and orientations show similar initial decay, but soon this decay is much slower and it saturates to a finite value for largest clusters, which is related to the velocity and the overall orientation of moving planar fronts.

Apart from the hydrodynamic and phoretic interactions, a different effect present in these systems is an additional inter-dimer alignment caused by the combination of self-propulsion and steric repulsion that we here refer to as *motility-induced attraction*. This alignment occurs since two rod-like propelling particles stay together longer than non-propelling ones. This effect is similar to

an effective attraction and it has been observed for elongated swimmers [42, 43]. To evaluate the importance of this effect, we perform Langevin Dynamics (LD) simulations, where hydrodynamics and phoretic effects are completely disregarded. Dimeric propelled particles are simulated by imposing driving forces that relate to swimming velocities comparable to those in the hydrodynamic simulations. Fluid friction is considered by an implicit solvent that we tune to lead to an effective viscosity very similar to the one in MPC-MD. Results are shown in Fig. 3 with dashed lines. Although some clustering is in fact also found in the LD simulations, these are mostly driven by simple collision events, and the average cluster orientation and velocity is clearly much smaller than in the MPC-MD ones. This proves that motility-induced attraction cannot be the cause of the observed swarming behavior. Instead, the observed swarming structures in the presence of a hydrodynamic solvent, especially those of the asymmetric dimers (see Fig. 1c), are due to the precise interplay of hydrodynamic and phoretic effects in these synthetic structures.

In the case of asymmetric dimeric swimmers where large clusters are formed, some of our simulations show percolated states in which a giant cluster extends over the whole simulation box. Upon percolation, almost all swimmers become part of one big, persistent planar and very fast front, with only little fluctuations. The appearance and stability of this giant front is a consequence of the periodic character of the employed boundary conditions. This means that it can be considered a simulation artifact and we have disregarded these realizations in our previous analysis and discussion. On the other hand, percolation has only been observed for asymmetric swimmers in a hydrodynamic solvent, what also highlights the strength of the lateral attraction in these swimmers. Furthermore, it is also important to note that the maximum size of our observed clusters is strongly limited by the size of our system; such a limitation does not exist in experimental systems. It is therefore reasonable to expect that very large and fast swarming clusters can be soon experimentally observed in systems of dimeric phoretic colloids.

In conclusion, we have shown that active thermophoretic asymmetric dimers assemble in moving clusters with flattened structures resulting from the interplay of hydrodynamics and phoresis. Although some swarming is also observed in symmetric thermophobic dimers, the stronger and longer ranged hydrodynamic interactions of the asymmetric active dimers makes that their clusters are considerably larger, faster, and more coherently oriented. This particular type of swarming can also be expected in other phoretic structures, such as catalytic dimeric swimmers with motion towards the non-catalytic surface. On the other hand, this behavior stands in contrast to most other artificial active systems based on spherical particles as well as to phoretically at-

tractive systems, where activity leads to clustering into unmoving structures. In systems of biological active particles, various ways of swarming have been described, although, to our knowledge, not in planar fronts as those here described. This novel phenomenology will broaden the scope of possible applications of active matter and offers intriguing new possibilities, for example in the design of microfluidic devices, or bio-compatible micromotors.

This work was supported by the DFG priority program SPP 1726 on “Microswimmers - from Single Particle Motion to Collective Behaviour”. The authors also gratefully acknowledge the computing time granted on the supercomputer JURECA at Jülich Supercomputing Centre (JSC).

-
- [1] W. F. Paxton, K. C. Kistler, C. C. Olmeda, A. Sen, S. K. St. Angelo, Y. Cao, T. E. Mallouk, P. E. Lammert, and V. H. Crespi, *J. Am. Chem. Soc.* **126**, 13424 (2004).
 - [2] R. Dreyfus, J. Baudry, M. L. Roper, M. Fermigier, H. A. Stone, and J. Bibette, *Nature* **437**, 862 (2005).
 - [3] J. Elgeti, R. G. Winkler, and G. Gompper, *Rep. Prog. Phys.* **78**, 056601 (2015).
 - [4] J. L. Anderson, *Ann. Rev. Fluid Mech.* **21**, 61 (1989).
 - [5] J. R. Howse, R. A. L. Jones, A. J. Ryan, T. Gough, R. Vafabakhsh, and R. Golestanian, *Phys. Rev. Lett.* **99**, 048102 (2007).
 - [6] L. F. Valadares, Y.-G. Tao, N. S. Zacharia, V. Kitaev, F. Galembeck, R. Kapral, and G. A. Ozin, *Small* **6**, 565 (2010).
 - [7] G. Loget and A. Kuhn, *Nature Comm.* **2**, 535 (2011).
 - [8] B. Sabass and U. Seifert, *J. Chem. Phys.* **136**, 214507 (2012).
 - [9] H. R. Jiang, N. Yoshinaga, and M. Sano, *Phys. Rev. Lett.* **105**, 268302 (2010).
 - [10] M. Yang and M. Ripoll, *Phys. Rev. E* **84**, 061401 (2011).
 - [11] K. Kroy, D. Chakraborty, and F. Cichos, *Eur. Phys. J. Special Topics* **225**, 2207 (2016).
 - [12] R. Kapral, *J. Chem. Phys.* **138**, 020901 (2013).
 - [13] M. Ibele, T. E. Mallouk, and A. Sen, *Angew. Chem. Int. Ed* **48**, 3308 (2009).
 - [14] J. Palacci, S. Sacanna, A. P. Steinberg, D. J. Pine, and P. M. Chaikin, *Science* **339**, 936 (2013).
 - [15] R. Golestanian, *Phys. Rev. Lett.* **108**, 038393 (2012).
 - [16] J. A. Cohen and R. Golestanian, *Phys. Rev. Lett.* **112**, 068302 (2014).
 - [17] B. Qian, D. Montiel, A. Bregull, F. Cichos, and H. Yang, *Chem. Sci.* **4**, 1440 (2013).
 - [18] L. Baraban, R. Streubel, D. Makarov, L. Han, D. Karnausenko, O. G. Schmidt, and G. Cuniberti, *ACS Nano* **7**, 1360 (2013).
 - [19] C. Lozano, B. ten Hagen, H. Löwen, and C. Bechinger, *Soft Matter* **7**, 12828 (2016).
 - [20] L. Soler, V. Magdanz, V. M. Fomin, S. Sanchez, , and O. G. Schmidt, *ACS Nano* **7**, 9611 (2013).
 - [21] D. Baigl, *Lab Chip* **12**, 3637 (2012).
 - [22] M. Yang and M. Ripoll, *Soft Matter* **12**, 8564 (2016).
 - [23] A. Malevanets and R. Kapral, *J. Chem. Phys.* **110**, 8605 (1999).
 - [24] R. Kapral, *Adv. Chem. Phys.* **140**, 89 (2008).
 - [25] Y.-G. Tao and R. Kapral, *Comput. Phys. Commun.* **10**, 770 (2009).
 - [26] D. Lüsebrink and M. Ripoll, *J. Chem. Phys.* **136**, 084106 (2012).
 - [27] M. Yang and M. Ripoll, *Soft Matter* **9**, 4661 (2013).
 - [28] T. Ihle and D. M. Kroll, *Phys. Rev. E* **67**, 066705 (2003).
 - [29] D. Lüsebrink, M. Yang, and M. Ripoll, *J. Phys.: Condens. Matter* **24**, 284132 (2012).
 - [30] J. T. Padding and A. A. Louis, *Phys. Rev. E* **74**, 031402 (2006).
 - [31] M. Wagner and M. Ripoll, *How to avoid depletion effects with the mpc method*, (preprint, 2016).
 - [32] M. Yang, A. Wysocki, and M. Ripoll, *Soft Matter* **10**, 6208 (2014).
 - [33] S. Plimpton, *J. Chem. Phys.* **117**, 1 (1995).
 - [34] M. K. Petersen, J. B. Lechman, S. J. Plimpton, G. S. Grest, P. J. in 't Veld, and P. R. Schunk, *J. Chem. Phys.* **132**, 174106 (2010).
 - [35] M. Braibanti, D. Vigolo, and R. Piazza, *Phys. Rev. Lett.* **100**, 108303 (2008).
 - [36] G. Volpe, I. Buttinoni, D. Vogt, H.-J. Kümmerer, and C. Bechinger, *Soft Matter* **7**, 8810 (2011).
 - [37] M. N. Popescu, M. Tasinkevych, and S. Dietrich, *EPL* **95**, 28004 (2011).
 - [38] S. Y. Reigh and R. Kapral, *Soft Matter* **11**, 3149 (2015).
 - [39] S. Thakur and R. Kapral, *Phys. Rev. E* **85**, 026121 (2011).
 - [40] See EPAPS Document No. [number will be inserted by publisher] for movies of the dynamics of thermophobic active colloidal dimers. For more information on EPAPS, see <http://www.aip.org/pubservs/epaps.html>.
 - [41] A. Zöttl and H. Stark, *Phys. Rev. Lett.* **112**, 118101 (2014).
 - [42] M. Abkenar, K. Marx, T. Auth, and G. Gompper, *Phys. Rev. E* **88**, 062314 (2013).
 - [43] F. Ginelli, F. Peruani, M. Bär, and H. Chaté, *Phys. Rev. Lett.* **104**, 184502 (2010).